Kinetics of Charge Separation and $A_0^- \rightarrow A_1$ Electron Transfer in Photosystem I Reaction Centers†

Sergei Savikhin,‡ Wu Xu,§ Peter Martinsson,|| Parag R. Chitnis,‡,§ and Walter S. Struve*,‡,||

Ames Laboratory−U.S. Department of Energy, Department of Chemistry, and Department of Biochemistry, Biophysics, and Molecular Biology, Iowa State University, Ames, Iowa 50011

Received February 28, 2001; Revised Manuscript Received June 12, 2001

ABSTRACT: The charge separation $P700^*A_0 \rightarrow P700^+A_0^-$ and the subsequent electron transfer from the primary to secondary electron acceptor have been studied by subtracting absorption difference profiles for cyanobacterial photosystem I (PS I) complexes with open and closed reaction centers. Samples were excited at 660 nm, which lies toward the blue edge of the core antenna absorption spectrum. The resulting PS I kinetics were analyzed in terms of the relevant P700, $P700^+$, A_0, and A_0^- absorption spectra. In our kinetic model, the radical pair $P700^+A_0^-$ forms with 1.3 ps rise kinetics after creation of electronically excited P700*. The formation of A_1^- via electron transfer from A_0^- requires ∼13 ps. The kinetics of the latter step are appreciably faster than previously estimated by other groups (20−50 ps).

All light-driven photochemistry in chlorophyll-containing photosynthetic organisms originates in reaction centers, pigment−protein complexes containing chlorophylloid molecules, quinones, and other cofactors. A dimeric special pair of chlorophylls within the reaction center receives electronic energy from the light-harvesting antenna pigments. This prompts a charge separation, creating an ionized special pair and a reduced primary electron acceptor. Subsequent electron transfers occur to a secondary electron acceptor and beyond, ultimately driving proton pumping and creation of electrical potentials across the photosynthetic membrane.

The sequence and timing of the primary events in reaction centers of purple photosynthetic bacteria have been well established for over a decade. The primary charge separation between the bacteriochlorophyll special pair (P) and the active bacteriopheophytin (H) occurs on the 2−3 ps time scale, yielding the radical pair P^+H^- (*1*). The electron transfer from H^- to the first quinone electron acceptor Q_A occurs in the low hundreds of picoseconds (*2*, *3*), while the subsequent electron transfer to the second quinone Q_B proceeds over still longer time scales. Such kinetic experiments, combined with the availability of X-ray structures (*4*, *5*) for reaction centers from the purple bacteria *Rhodobacter sphaeroides* and *Rhodopseudomonas viridis*, prompted a flood of mutational and theoretical studies on their structure−function relationships.

The question arises as to whether the primary processes in photosystem I (PS I)[1] reaction centers resemble those in purple bacterial reaction centers, given the coarse similarity in their cofactor arrangements (*4*−*7*). The only PS I reaction center with known 3-dimensional structure is that from the cyanobacterium *Synechococcus elongatus* (*6*, *7*). The pigment arrangement is similar to that in purple bacterial reaction centers: it comprises the P700 special pair Chls, two Chls that are analogous to the accessory Bchls in purple bacteria, and two Chls in positions reminiscent of the BPheos. One or both of the latter two Chls is believed to function as the primary electron acceptor A_0. While electron transfer occurs preferentially in the L branch in wild-type purple bacterial reaction centers, it has not been established whether one or both branches (PsaA or PsaB) are active in PS I. The center-to-center distances among the six reaction center chlorophylls in PS I resemble those among the corresponding pigments in the bacterial systems (*7*). However, the ∼80 kDa PsaA and PsaB protein subunits which coordinate the PS I reaction center cofactors also bind ∼100 core antenna chlorophylls (*6*); spectral overlap with the redmost antenna chlorophylls precludes selective excitation of reaction center chlorophylls in flash kinetic studies. The presence of antenna pigments and spectral congestion among reaction center cofactors has similarly precluded facile kinetic studies of photosystem II reaction centers (*8*). The large PS I core antenna size exacerbates exciton annihilation artifacts, and limits pumping densities to excitation of <1 pigment out of 300 (*9*). Hastings et al. (*10*) proposed a strategy for isolating the reaction center kinetics by obtaining time-resolved absorption difference profiles for PS I core complexes with open and closed reaction centers. (In the following, the terms "open" and "closed" refer to reaction centers containing P700 and $P700^+$, respectively. This convention differs from one commonly

† Research at Ames Laboratory was supported by the Division of Chemical Sciences, Office of Basic Energy Sciences, U.S. Department of Energy. Ames Laboratory is operated by Iowa State University under Contract W-7405-Eng-82. Generation of the PS I mutants was supported by NSF Grants to P.R.C. (MCB 970023 and 0078264). Ultrafast experiments were supported by the Ames Laboratory; steady-state measurements were performed under NSF Grant MCB 9904612 (to W.S.S.).

* To whom correspondence should be addressed. Fax: (515) 294 1699. E-mail: wstruve@ameslab.gov.

‡ Ames Laboratory−U.S. Department of Energy.

§ Department of Biochemistry, Biophysics, and Molecular Biology.

|| Department of Chemistry.

[1] Abbreviations: A_0, chlorophylloid primary electron acceptor; A_1, phylloquinone secondary acceptor; (B)Chl, (bacterio)chlorophyll; BPheo, bacteriopheophytin; P700, special pair Chls; PS I, photosystem I.

10.1021/bi0104165 CCC: $20.00
Published on Web 07/13/2001

used in PS II work, where the same terms refer to the oxidation state of the secondary electron acceptor rather than that of the special pair.) Since extensive evidence suggests that the antenna kinetics are unaffected by the P700 oxidation state (*11*−*16*), the difference between the absorption difference profiles for open and closed reaction centers should isolate the reaction center processes. [To emphasize that these (open − closed) difference profiles are actually difference−difference profiles, the vertical coordinates in the figures displaying them are labeled "ΔΔ*A*". The same remark applies to (open − closed) absorption difference spectra.] To our knowledge, there is no physical reason a priori why P700 and $P700^+$ should quench antenna excitation in exactly the same manner. Byrdin et al. (*17*) reported that the antenna excitation decay kinetics differ by ∼10% in the presence of open and closed reaction centers in PS I from *Synechococcus elongatus*. Such a difference would not be negligible in the present experiments, because the absorption difference signals to be subtracted are considerably larger than the (open − closed) absorption difference signal. However, Savikhin et al. (*16*) recently showed that for the cyanobacterium *Synechocystis* sp. PCC 6803, the kinetics of antenna excitation trapping at P700 and $P700^+$ are much more similar, differing by 1−2% (23.6 vs 24.0 ps). In earlier work (*9*), we reported that the antenna kinetics for PS I with open reaction centers differed from those for PS I with closed reaction centers, in that a decay-associated spectral (DAS) component with lifetime 6−7 ps was present for closed reaction centers, but was absent for open reaction centers. Our intervening experience shows that this difference actually stems from contrasting *reaction center* (rather than antenna) processes in complexes with open and closed reaction centers. Much of the DAS amplitude in this 6−7 ps global component is concentrated in the spectral region of the A_0 and P700 reaction center cofactors (*9*). Local biexponential fits to (open − closed) difference profiles probed at 690 nm yield apparent components with lifetimes of 6−10 and 20−24 ps (*16*). We show here that such difference profiles can be accounted for in terms of P700* → $P700^+A_0^-$ charge separation and A_0^- → A_1 electron-transfer kinetics, using realistic reaction center cofactor spectra.

In this work, we have studied these reaction center events by analyzing ultrafast (open − closed) absorption difference profiles for PS I excited at 660 nm, and probed at several wavelengths (675−720 nm) that bracket the main absorption features of the key reaction center cofactors. This allows independent determination of the time scales for the overall charge separation P700*A_0 → $P700^+A_0^-$ and the electron transfer from primary to secondary electron acceptor in PS I.

MATERIALS AND METHODS

Trimeric PSI complexes were purified from the wild-type strain of the cyanobacterium *Synechocystis* sp. PCC 6803 by a previously published method (*18*). Optical clarity of the PS I preparation was improved by centrifugation through Spin-X centrifuge filter units (0.22 μm cellulose acetate membrane; Costar). The chlorophyll concentration of PSI trimers was measured in 80% acetone. Purity of PSI preparations was examined by SDS−PAGE analysis of protein subunits. All PS I samples in the ultrafast measurements contained 20 mM sodium ascorbate. As demonstrated by Savikhin et al. (*16*), samples in experiments conducted in total darkness contained predominantly open reaction centers, which contain unoxidized P700. Continuous-wave (cw) illumination of the sample cell with a 3 V flashlight bulb yielded samples in which the reaction centers were almost exclusively closed (i.e., containing $P700^+$). Under these conditions, electron recombination with $P700^+$ occurs with 120 s kinetics in 20 mM ascorbate; this is orders of magnitude slower than the normal 45 ms recombination between $P700^+$ and the reduced terminal acceptors $F_{A/B}^-$ (*19*). This fact, combined with our observation that the recombination rate is proportional to ascorbate concentration (S. Savikhin, W. Xu, P. R. Chitnis, and W. S. Struve, unpublished work), indicates that the 120 s recombination occurs directly from the ascorbate, rather than from $F_{A/B}^-$. Pulsed light excitation efficiently generates $P700^+F_{A/B}^-$, but a fraction of the electrons on the terminal electron acceptors are then scavenged from the PS I complex (*20*) before recombination can occur from $F_{A/B}^-$. Several seconds of cw illumination thus cause population buildup in PS I complexes with closed reaction centers. This fact greatly facilitates accumulation of (open − closed) absorption difference profiles in PS I, because the required light gating for preparing open and closed reaction centers is shifted from milliseconds to seconds. It obviates the need for three-pulse pump−probe experiments, in which PS I reaction centers are closed with an intense preflash before introducing pump and probe pulses within ≪45 ms. Our ability to interchange open and closed reaction centers without changes in sample or beam geometry ensured exact mutual normalization of the respective pump−probe profiles for subtraction.

The optical pump−probe spectroscopy system has been described in detail elsewhere (*9*, *16*). Pulses from a self-mode-locked Ti:sapphire laser were amplified by a factor of $\sim 10^6$ at 1 kHz repetition rate in a regenerative amplifier. The 780 nm output was recompressed to ∼90−100 fs duration using a grating pair, and converted to infrared signal and idler pulses in a Type I BBO optical parametric amplifier (*21*). The signal output pulses were frequency-doubled into tunable visible light pulses (600−730 nm), which served as sample excitation pulses. Sample absorption was probed with broadband continuum light pulses generated in a sapphire plate; cross-correlations between the pump and probe pulses were typically 100−200 fs fwhm. Wavelength dispersion in the pump−probe cross-correlation functions (e.g., arising from continuum pulse chirp) was carefully checked at each probe wavelength. Continuum pulses were split into signal and reference beams, dispersed in an Oriel MS257 imaging monochromator operated at ∼3 nm band-pass, and directed onto separate Hamamatsu S3071 Si pin photodiodes. The pump intensity was monitored and digitized, along with the transmitted signal and reference beams. This permitted digital filtering, whereby noise spikes (e.g., arising from dust in the sample) were eliminated; this improved the signal/noise ratio by factors of up to 10 for turbid samples. It also provided for real-time noise monitoring, an important tool for optimal alignment of the pump−probe optics. Noise performance was near shot noise-limited; the rms noise in *dA* was $\sim 10^{-5}$ for 1 s accumulation time.

Operation in the annihilation-free regime was ensured by control experiments in which the pump power was varied; all experiments were performed at room temperature. PS I

samples exhibited ~0.3 optical density at 660 nm, and were housed in a spinning cell with 0.7 mm path length; the excitation density was ~1.5 μJ/cm^2 (1.5 nJ/pulse, ~300 μm spot size). This yielded excitation of 1 out of every ~1000 Chls. The pump and probe polarizations were separated by 54.7°, to exclude anisotropy effects in the measured kinetics.

RESULTS

Absorption Spectra of P700 and P700$^+$. Oxidation of the P700 special pair in PS I reaction centers generates a monomeric chlorophyll cation (Chl$^+$) and a neutral monomeric Chl (C690) that absorbs at ~690 nm (*22*). Chl$^+$ is responsible for a very broad absorption band centered near 800 nm; this band is frequently monitored in studies of electron transfers between PS I and cytochromes and plastocyanins (*23*, *24*). The width of the narrower (~10 nm fwhm) C690 Q_y origin band is characteristic of monomeric Chl pigments in protein environments. The oxidized P700$^+$ spectrum (whose components are the Chl$^+$ and C690 spectra) is strongly dominated by the C690 origin band in the spectral range probed in the present experiments (675−720 nm). The P700 absorption spectrum in open reaction centers exhibits ~30 nm fwhm, which is typical of charge-transfer transitions in dimeric Chls (*25*). After charge separation and reduction of the secondary electron acceptor A_1, the P700 absorption spectrum is bleached, and is supplanted by the P700$^+$ spectrum; by this time, the primary electron acceptor A_0 reverts to its original neutral state. Since the phylloquinone A_1 and the remaining cofactors in the electron-transfer chain (the 4Fe-4S centers F_X and $F_{A/B}$) do not absorb in the visible, the subsequent reaction center events are not expected to cause further absorption changes between 675 and 720 nm. On these grounds, Savikhin et al. (*16*) reasoned that the PS I (open − closed) absorption difference spectrum at long times should evolve into the steady-state (P700$^+$ − P700) absorption difference spectrum, which can be measured in a conventional spectrophotometer. They further assumed that all of the (open − closed) difference spectral changes arising from events leading to creation of P700$^+$A$_1^-$ could be modeled in terms of population-weighted P700 and P700$^+$ spectra; the spectra themselves were derived from a multiple Gaussian fit to the steady-state (P700$^+$ − P700) spectrum. This procedure ignored P700* stimulated emission as well as the contributions from A_0 photobleaching and recovery; the latter contributions accompany reduction and reoxidation of A_0, and would be negligible if rapid $A_0^- \rightarrow A_1$ electron transfer precluded significant population buildup of A_0^-.

In the present work, the transient P700 and P700$^+$ spectra were measured directly for use in the kinetic analysis. Absorption difference spectra were accumulated by exciting wild-type PS I samples at 660 nm, and sweeping the probe wavelength at fixed time delay (200 ps). The resulting profile for closed reaction centers was subtracted from that for open reaction centers; mutual normalization was ensured, because quantitative interconversion between P700 and P700$^+$ was achieved without changes in optical geometry or sample absorption at 660 nm (cf. Materials and Methods). This 200 ps (open − closed) absorption difference spectrum is shown in the top panel of Figure 1, along with the steady-state (P700$^+$ − P700) difference spectrum. These spectra resemble (P700$^+$ − P700) absorption difference spectra that have been reported by other researchers (e.g., *11*, *22*, *26*). Several

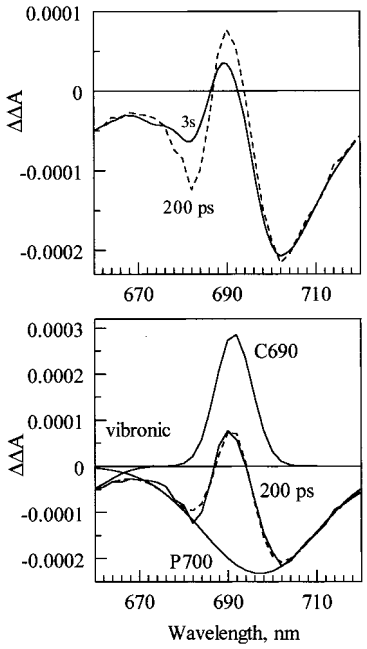

FIGURE 1: Top panel: Experimental (open − closed) absorption difference spectrum at 200 ps for PS I complexes from *Synechocystis* sp. excited at 660 nm (dashed curve); steady-state (P700$^+$ − P700) absorption difference spectrum (solid curve). The steady-state spectrum is labeled "3s", because it was recorded after 3 s continuous-wave illumination (see Materials and Methods). Bottom panel: Gaussian spectral components for P700 bleaching and C690 absorption, derived from analysis of the 200 ps (open − closed) absorption difference spectrum at 200 ps. Curves labeled "200 ps" are the experimental absorption difference spectrum (solid curve) and the optimized multiple Gaussian fit (dashed curve). Vibronic components were included in order to fit the experimental spectrum at wavelengths shorter than 670 nm; kinetic analysis only includes wavelengths ≥675 nm. Negative-going signals indicate photobleaching/stimulated emission; absorption difference scales are absolute under the present experimental conditions.

groups have reported that the $A_0^- \rightarrow A_1$ electron transfer occurs within 20−50 ps. Since 200 ps is several times longer than this, the two spectra in the top of Figure 1 should be similar. The spectra are not identical; the principal difference stems from the fact that the C690 spectrum broadens slightly between 200 ps and 3 s without significant spectral shifting. In separate experiments (not shown), the kinetics of this spectral diffusion were shown to be ~300 ns; the likely origin of this process is protein motions in the neighborhood of C690 following creation of P700$^+$. Since band-shifting is not a major component in the observed C690 spectral evolution, electrochromic effects do not appear to be dominant here. A Gaussian decomposition of the 200 ps (open − closed) difference spectrum was used to obtain the P700 and P700$^+$ spectral parameters for analysis of the present kinetic experiments. The resulting Gaussian components for C690 absorption and P700 bleaching are shown in the bottom panel of Figure 1, along with the experimental and fitted 200 ps (open − closed) difference spectrum. The optimized parameters for the P700 photobleaching component in this difference spectrum are 697.1 nm band position, 30.4 nm width (fwhm), and amplitude −0.00034 (in absolute absorption difference units). For the C690 absorption band, the respective parameters are 691.4 nm, 9.7 nm, and +0.00041; for Chl$^+$, they are 800 nm, 82 nm, and +0.00005. (The Chl$^+$ component exhibits very small amplitudes in the wavelength range of Figure 1.) The vibronic bands that gain

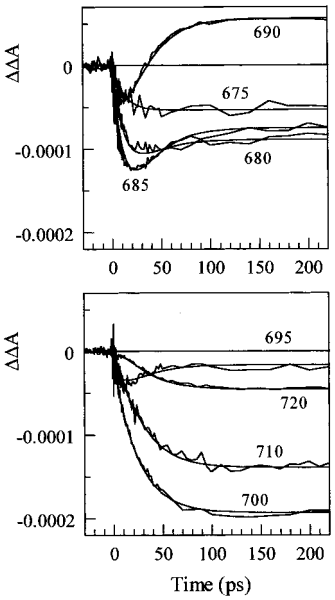

FIGURE 2: Time-resolved (open − closed) absorption difference profiles for PS I complexes excited at 660 nm, and probed at the indicated wavelengths in nanometers. Noisy curves are experimental. Smooth curves are optimized fits with eq 1, using the lifetimes τ_2 and τ_3 and Gaussian spectral parameters for A_0 and A_0^- as variables. The lifetime τ_1 was fixed at 23 ps; optimal values for the other lifetimes were $\tau_2 = 1.3$ ps and $\tau_3 = 13$ ps. Negative-going signals indicate photobleaching/stimulated emission; absorption difference scales are absolute under the present experimental conditions.

importance at shorter wavelengths were not included in the kinetic analysis, which did not extend to wavelengths shorter than 675 nm (see below).

Time-Resolved Kinetics. Figure 2 shows (open − closed) time-resolved absorption difference profiles obtained for wild-type PS I complexes excited at 660 nm, and probed at eight wavelengths from 675 to 720 nm. All of these profiles were simultaneously fitted with the absorption difference signal

$$S(\lambda,t) = (\epsilon_{P700+} - \epsilon_{P700}) + \left[-\frac{\tau_2}{\tau_1-\tau_2}(\epsilon_{P700} + s_{P700*}) + \frac{\tau_3\tau_1}{(\tau_1-\tau_2)(\tau_1-\tau_3)}(\epsilon_{P700+} - \epsilon_{P700} - \epsilon_{A0} + \epsilon_{A0-}) - \frac{\tau_1^2}{(\tau_1-\tau_2)(\tau_1-\tau_3)}(\epsilon_{P700+} - \epsilon_{P700})\right]e^{-t/\tau_1} + \left[\frac{\tau_2}{\tau_1-\tau_2}(\epsilon_{P700} + s_{P700*}) - \frac{\tau_3\tau_2}{(\tau_1-\tau_2)(\tau_2-\tau_3)}(\epsilon_{P700+} - \epsilon_{P700} - \epsilon_{A0} + \epsilon_{A0-}) - \frac{\tau_2^2}{(\tau_2-\tau_1)(\tau_2-\tau_3)}(\epsilon_{P700+} - \epsilon_{P700})\right]e^{-t/\tau_2} + \left[\frac{\tau_3^2}{(\tau_1-\tau_3)(\tau_2-\tau_3)}(\epsilon_{P700+} - \epsilon_{P700} - \epsilon_{A0} + \epsilon_{A0-}) - \frac{\tau_3^2}{(\tau_3-\tau_1)(\tau_3-\tau_2)}(\epsilon_{P700+} - \epsilon_{P700})\right]e^{-t/\tau_3} \quad (1)$$

that is consistent with the phenomenological sequence of first-order steps:

$$\text{Antenna*P700 } A_0\ A_1 \xrightarrow[\tau_1]{} \text{Antenna P700* } A_0\ A_1 \xrightarrow[\tau_2]{} \text{Antenna P700}^+\ A_0^-\ A_1 \xrightarrow[\tau_3]{} \text{Antenna P700}^+\ A_0\ A_1^-$$

In this model, the asterisk denotes electronic excitation. The lifetime τ_1 corresponds to antenna excitation trapping at P700, τ_2 represents the overall charge separation $P700^*A_0 \rightarrow P700^+A_0^-$, and τ_3 represents the $A_0^- \rightarrow A_1$ electron transfer. The validity of this kinetic model is analyzed under Discussion (see below). The experimental trapping time τ_1 is ~23 ps in wild-type *Synechocystis* sp. (*16*); it encompasses the cumulative effects of antenna excitation equilibration, trapping at P700, and back-transfers from P700 to the antenna (see Discussion). The P700 and $P700^+$ absorption spectra $\epsilon_{P700}(\lambda)$ and $\epsilon_{P700^+}(\lambda)$ are known from analysis of the 200 ps (open − closed) absorption difference spectrum (previous section). The unknown parameters in eq 1 are the lifetimes τ_2 and τ_3 for the $P700^* \rightarrow A_0$ and $A_0^- \rightarrow A_1$ electron-transfer steps, the A_0 and A_0^- absorption spectra $\epsilon_{A0}(\lambda)$ and $\epsilon_{A0^-}(\lambda)$, and the P700* stimulated emission spectrum $s_{P700*}(\lambda)$. No stimulated emission terms are included for $P700^+$, A_0^-, or A_1^-, charged species which appear in their electronic ground states.

The P700* stimulated emission spectrum was represented by a symmetric Gaussian function of the same width and amplitude as $\epsilon_{P700}(\lambda)$. In a spectral hole-burning study of the primary donor state of PS I reaction centers from spinach at 1.6 K, Gillie et al. (*25*) determined that while the P700 absorption peak lies at ~702 nm, the zero-point level (ZPL) occurs at 710 nm. The P700 absorption spectrum can be modeled using a mean phonon frequency in the range 35−50 cm^{-1} with Huang−Rhys factor $S = 4-6$. To first order, the P700* stimulated emission spectrum would resemble the P700 absorption spectrum reflected through the ZPL, if complete vibrational relaxation occurs before P700* is probed. For a symmetric Gaussian P700 band, this reflection would be equivalent to a red shift by twice the separation between the ZPL and the P700 band maximum. However, P700* is initially generated with a distribution of excess vibrational energies arising from energy transfers from neighboring antenna Chls; most of the latter have ZPL's at wavelengths <695 nm. [This situation differs fundamentally from that in purple bacterial reaction centers, whose kinetics were studied by directly exciting the primary donor state (*1*).] The resulting P700* stimulated emission spectrum would depend on the extent of relaxation in the spectrally active vibrational mode(s) during its lifetime. The theoretical P700* stimulated emission spectrum from a specific vibrational level can be modeled using Franck−Condon factors for displaced harmonic oscillators. Aside from the fact that the vibrationally summed Einstein coefficients must be equal for absorption and stimulated emission, these unrelaxed spectra would not resemble the P700 absorption spectrum. For example, the most intense vibrational band in the P700* stimulated emission spectrum from the level(s) corresponding

to the absorption band maximum λ_0 (=697.1 nm in *Synechocystis* sp.) would occur at λ_0. This spectrum would fade to the red ($\lambda > \lambda_0$), and would be clipped for most wavelengths $\lambda < \lambda_0$. Since the relevant P700* vibrational distribution is unknown during the P700* lifetime, its stimulated emission spectrum $s_{P700*}(\lambda)$ was represented ad hoc by a symmetric Gaussian of fixed width and height, plus a variable shift parameter. Finally, the A_0 and A_0^- spectra were represented by single symmetric Gaussians with variable position, amplitude, and width.

In our initial analysis, the amplitude of the A_0 absorption spectrum was set equal to that of the C690 spectrum. The other A_0 and A_0^- spectral parameters were free, as were the lifetimes τ_2 and τ_3. The shift between the P700 absorption and P700* stimulated emission spectral peaks was frozen at zero. Figure 2 shows the resulting fits of eq 1 to the experimental pump−probe profiles. The optimized parameters for the A_0 Gaussian peak were position 685.1 nm, width 12.4 nm, and amplitude 0.00041 (the latter is identical to that of C690, see above); and for the A_0^- component, position 717.1 nm, width 24.9 nm, and amplitude 0.000125. Our optimized position and width for the A_0 spectrum resemble those reported by several other groups (*10*−*12*). The inclusion of an A_0^- absorption spectrum in eq 1 is necessary for good fits, particularly at the longest probe wavelengths (see below). The position and amplitude of the A_0^- spectrum are not well-defined in this analysis, because it only partially overlaps the spectral range of our experiments. Previous measurements (*27*) of the steady-state (Chl^- − Chl) absorption difference spectrum for monomeric Chl in DMF suggest the presence of a broad Chl^- absorption peak between 700 and 800 nm. Finally, the optimized lifetimes obtained in this analysis are $\tau_2 = 1.3$ ps and $\tau_3 = 13$ ps. The first of these corresponds to the kinetics of A_0^- formation, while the second describes the formation of A_1^-.

In separate fits that allowed the P700* stimulated emission band position to vary, the optimized shift from the P700 spectrum was zero, suggesting that the P700* stimulated emission is unrelaxed. However, this stimulated emission component only influenced fits during the earliest 1−2 ps of the 200 ps window in Figure 2 (see below), so that details of the P700* stimulated emission spectrum are relatively unimportant to the overall fits during the 200 ps time window of Figure 2.

As a check on our A_0 and A_0^- spectra, the (open − closed) absorption difference spectrum was accumulated at 8 ps. At this time delay, reduction of the secondary electron acceptor A_1 is incomplete, and contributions are expected from the absorption features due to A_0 and A_0^-. This spectrum (shown in Figure 3) was fitted using eq 1. The lifetime parameters were fixed at $\tau_1 = 23$ ps, $\tau_2 = 1.3$ ps, and $\tau_3 = 13$ ps; all of the A_0 and A_0^- Gaussian parameters (including amplitudes) were allowed to vary. The $P700^+$ spectrum (which combines the P700 bleaching and C690 absorption features with parameters determined in the analysis of Figure 1) was represented as the 200 ps spectrum weighted by a factor of 0.27. This factor, which equals the amount of $P700^+$ formed at 8 ps relative to that present at 200 ps according to our kinetic model, is very close to exp(−8/23). P700* stimulated emission was represented as before, with the P700* population weight determined by the kinetic model (1.2% of the total excitations at 8 ps). The resulting A_0 absorption band

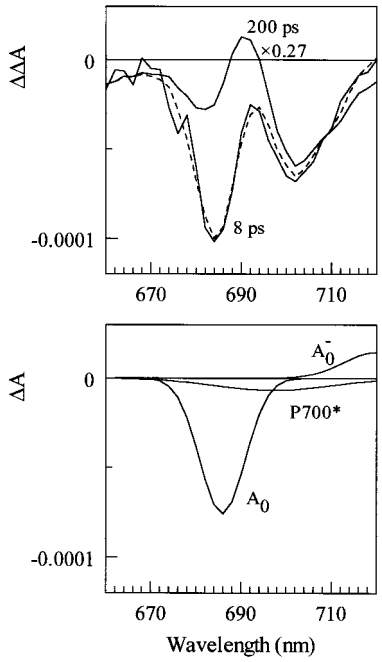

FIGURE 3: Top panel: (Open − closed) absorption difference spectra at 8 and 200 ps. The 200 ps spectrum is scaled by a factor of 0.27 [approximately exp(−8/23); see text] for direct comparison to the 8 ps spectra. Solid curves are experimental; the dashed curve is the best fit to the experimental 8 ps profile using eq 1, with A_0 and A_0^- Gaussian spectral parameters as variables. Bottom panel: Gaussian components for A_0 bleaching and A_0^- absorption at 8 ps, derived from the best fit of eq 1 to the 8 ps difference spectrum; and the P700* stimulated emission spectrum at 8 ps. The sum of these three curves comprises the modeled difference between the 8 ps and scaled 200 ps spectra in the upper panel.

exhibited 11 nm fwhm, and was centered at 685.7 nm; its amplitude was larger than that of C690 by a factor of 1.05. The A_0^- spectrum, which emerges at 706 nm with 33 nm fwhm, qualitatively resembles the one yielded by the prior analysis. This A_0 spectrum conforms closely to the one obtained by analysis of the time-resolved profiles in Figure 2. The bottom panel of Figure 3 shows the resulting Gaussian components that describe the main A_0 bleaching and A_0^- absorption bands. The best fit to the 8 ps (open − closed) absorption difference spectrum is superimposed on the experimental spectrum in the top panel of Figure 3.

As an additional check, the absorption spectrum of the primary electron acceptor A_0 was also derived from the 200 ps (open − closed) difference spectrum for a *menB* mutant PS I from *Synechocystis* sp. In this mutant (*28*), interruption of the *menB* gene disables the biosynthesis of phylloquinone (A_1); the A_1 binding pocket is then occupied by 9-plastoquinone, which is ordinarily found elsewhere in the photosynthetic apparatus. The PS I protein subunits in this mutant exhibit no genetic differences from those in the wild type. The steady-state ($P700^+$ − P700) absorption difference spectrum of *menB* PS I nearly coincides with that in the wild type, and the *menB* antenna kinetics are very similar to those in the wild type (not shown). However, the electron transfer from A_0^- to A_1 in *menB* PS I is far slower (>5 ns) than in the wild type (S. Savikhin, W. Xu, P. Martinsson, P. R. Chitnis, and W. S. Struve, unpublished work). The $A_1^- \rightarrow F_X$ electron transfer is similarly decelerated in this mutant (*29*). Hence, the 200 ps *menB* (open − closed) difference spectrum between 680 and 700 nm is expected to differ from

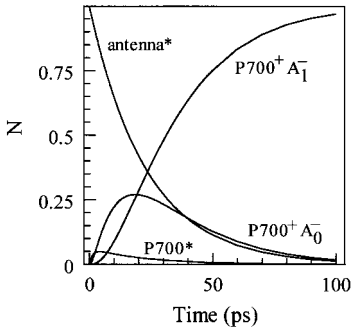

FIGURE 4: Optimized time-dependent state populations from analysis of absorption difference kinetics in Figure 2 using eq 1, with $\tau_1 = 23$ ps, $\tau_2 = 1.3$ ps, and $\tau_3 = 13$ ps. Populations are normalized so that the initial antenna excited state population is unity.

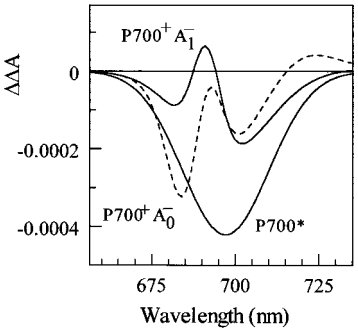

FIGURE 5: Modeled absorption difference spectra for the states P700*, $P700^+A_0^-$, and $P700^+A_1^-$. The latter spectrum is the optimized fit to the 200 ps (open − closed) absorption difference spectrum.

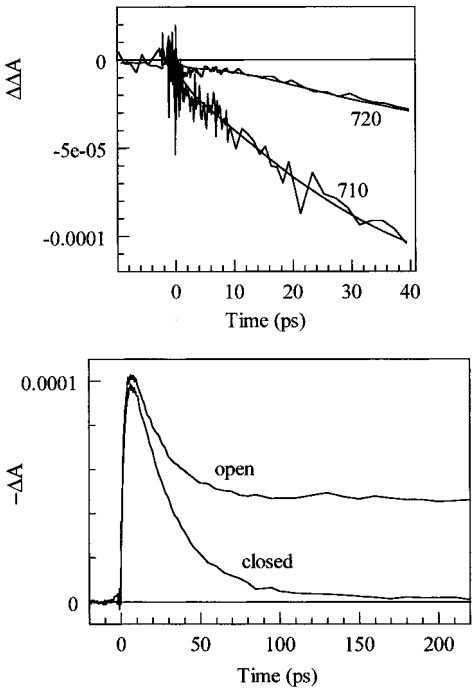

FIGURE 6: Top panel: Time-resolved (open − closed) absorption difference profiles excited at 660 nm, and probed at 710 and 720 nm. Negative-going signals correspond to photobleaching/stimulated emission. Bottom panel: Individual time-resolved profiles for PS I with open and closed reaction centers probed at 720 nm; time window is 200 ps. Signals for open and closed reaction centers are essentially congruent for times <2 ps; significant differences develop for times >10 ps. Positive-going signals correspond to photobleaching/stimulated emission.

the corresponding wild-type difference spectrum primarily through the appearance of an (A_0^- − A_0) spectral component, arising from quantitative reduction of A_0. The 200 ps *menB* difference spectrum was fitted as a sum of a single Gaussian A_0 photobleaching band near 685 nm, a broad A_0^- absorption band with low amplitude extending to the far red, and the wild-type 200 ps difference spectrum multiplied by a variable scaling factor. The resulting A_0 spectrum is centered at 686.6 nm, and exhibits ~12 nm fwhm; in this analysis, the absolute ratio of A_0 to C690 amplitudes was 1.07. These A_0 spectral parameters closely resemble the ones obtained by fitting the 8 ps (open − closed) difference spectrum in wild-type PS I (Figure 3). This corroborates our assignments of the Gaussian parameters for the main A_0 absorption band.

The importance of A_0^- absorption growth in our fits at the longest wavelengths is illustrated in Figures 4 and 5. Figure 4 shows the time-dependent populations for the sequence of states P700*, $P700^+A_0^-$, and $P700^+A_1^-$ yielded by our analyses of the time-resolved (open − closed) profiles in Figure 2. These are normalized so that the initial population of antenna* is unity. The optimized absorption difference spectra corresponding to these populations are shown in Figure 5; they are given by $-(\epsilon_{P700} + s_{P700*})$, $-(\epsilon_{P700} - \epsilon_{P700^+} + \epsilon_{A0} - \epsilon_{A0^-})$, and $-(\epsilon_{P700} - \epsilon_{P700^+})$, respectively. During the first ~5 ps, the populations of P700* and $P700^+A_0^-$ grow nearly apace (Figure 4), while the values of the corresponding absorbance changes at 720 nm are nearly equal but opposite in sign (Figure 5). The total absorption difference signal at 720 nm (top panel of of Figure 6) therefore remains anomalously close to zero for the first few picoseconds. It is only at times >10 ps (when the A_0^- population decays due to $A_0^- \rightarrow A_1$ electron transfer) that the empirical photobleaching growth begins. In contrast, the photobleaching rise feature in the 710 nm pump−probe profile initiates at ~0 ps. The bottom panel of Figure 6 (which gives the individual pump−probe profiles at 720 nm for open and closed reaction centers in three time windows) shows that the unusual behavior at 720 nm is not an artifact of time-shifting, e.g., caused by wavelength dispersion in the continuum probe optics. The rise features in the pump−probe signals at times <2 ps for open and closed reaction centers superimpose almost exactly; significant differences between the open and closed profiles only develop at times >10 ps. This example emphasizes the importance of including an A_0^- component in the overall kinetic fits using eq 1.

At times later than ~5 ps, the contribution of the P700* stimulated emission to the absorption difference spectrum is insignificant relative to those of P700 bleaching and C690 absorption. By 8 ps, the PS I (open − closed) absorption difference spectrum is distinguished from the 200 ps difference spectrum primarily through the presence of a (A_0^- − A_0) component; P700* stimulated emission has become negligible by comparison. Inclusion of the P700* stimulated emission terms in eq 1 therefore drives the time constant τ_2 for the P700* → $P700^+A_0^-$ charge separation into the regime of ~1 ps or less. In the perspective of Figure 4, the P700* population peaks at 3−4 ps, and is then quickly overtaken by that of $P700^+A_0^-$; it never surpasses 5% of the original antenna excitation population. This justifies one of our derivations of the (A_0^- − A_0) difference spectrum, based on fitting our 8 ps (open − closed) absorption difference spectrum as a combination of the 200 ps absorption differ-

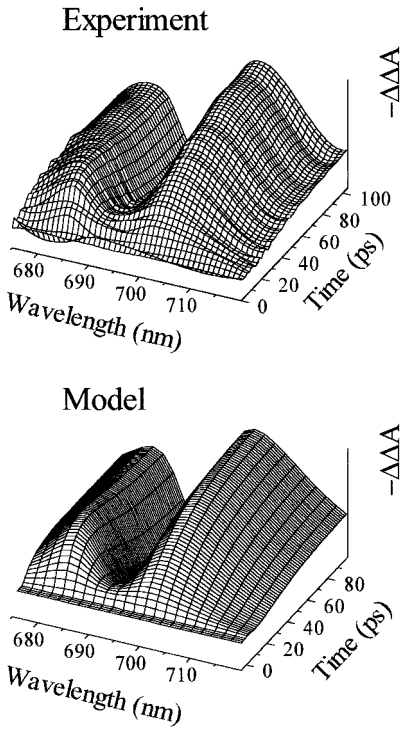

FIGURE 7: Time evolution of (open − closed) absorption difference spectra for PS I excited at 660 nm: experimental (top) and optimized fit to kinetic model (bottom). The eight probe wavelengths in the experimental surface were augmented using a cubic spline to facilitate comparison with the model suface. The vertical coordinate is the absorption difference signal; for ease of visualization, positive signals correspond to photobleaching/stimulated emission.

ence spectrum (P700 bleaching plus C690 absorption) with Gaussian bands representing A_0 bleaching and A_0^- absorption.

The confidence intervals for the lifetimes τ_2 and τ_3 were studied by fixing τ_1 and either τ_2 or τ_3 at their optimized values, and varying the other lifetime in fits analogous to those in Figure 2. For the $A_0^- \rightarrow A_1$ transfer time τ_3, values between 8 and 14 ps provided reasonable fits to the experimental profiles within noise. Beyond these limits, the fitted profiles deviated from experimental beyond noise. By the same criterion, values of τ_2 equal to or less than 3 ps provided reasonable fits. Hence, the error bounds on these lifetimes in our model are $\tau_2 \leq 3$ ps, and 8 ps $< \tau_3 <$ 14 ps.

Figure 7 compares the experimental and fitted 3-dimensional surfaces for the (open − closed) absorption difference signals versus time and probe wavelength.

DISCUSSION

The sequence of irreversible first-order steps in the kinetic model of eq 1 appears oversimplified a priori, because the overall excitation trapping at P700 arises from multiple sequences of reversible energy transfers. The bulk of the absorption at 660 nm (the excitation wavelength used in the time-resolved experiments) occurs in antenna Chls. Some excitation is deposited in Chls with Q_y 0−0 bands near 660 nm; some is absorbed in vibronic features of the numerous Chls with 0−0 bands at significantly longer wavelengths (670−695 nm). Minimal pump light is directly absorbed by reaction cofactors such as P700 or A_0. Much of the ensuing equilibration among the bulk antenna Chls shows kinetics in the hundreds of femtoseconds; equilibration between the bulk antenna and the far-red antenna Chls C708 and C714 in *Synechocystis* sp. (*30*) requires ∼2 ps (*16*). P700* can be created through a panoply of pathways; these include direct energy transfers from nearby core antenna Chls, as well as indirect routes passing through A_0, the "connecting" Chls, and/or the accessory Chls. Back-transfers can also occur between P700* and the surrounding Chls. Hence, even if the empirical antenna excitation (antenna*) population decay can be well described using single-exponential kinetics with lifetime τ_1, and even if the charge separation and the $A_0^- \rightarrow A_1$ electron transfer are essentially irreversible, it is not immediately obvious that the population kinetics for P700*, $P700^+A_0^-$, or $P700^+A_1^-$ should conform to the analytical expressions

$$N_{P700^*}(t) = \frac{\tau_2}{\tau_1 - \tau_2}(e^{-t/\tau_1} - e^{-t/\tau_2})$$

$$N_{P700+A0-}(t) = \frac{\tau_1\tau_3}{(\tau_1 - \tau_2)(\tau_1 - \tau_3)}e^{-t/\tau_1} + \frac{\tau_2\tau_3}{(\tau_1 - \tau_2)(\tau_3 - \tau_2)}e^{-t/\tau_2} + \frac{\tau_3^2}{(\tau_3 - \tau_1)(\tau_3 - \tau_2)}e^{-t/\tau_3} \quad (2)$$

$$N_{P700+A1-}(t) = 1 - e^{-t/\tau_1} - N_{P700^*} - N_{P700+A0-}$$

that are embodied in the kinetic model of eq 1.

More detailed simulations show that eqs 2 nevertheless do provide a highly accurate representation of the PS I kinetics. In the simplest simulation, the model underlying eq 1 was augmented with a single back-transfer channel from P700* to the antenna. The lifetimes τ_2 and τ_3 were fixed at 1.3 and 13 ps, respectively; the lifetime τ_b for back-transfer was fixed at values ranging from 0.5 to 5 ps; and the rate for the forward antenna* → P700 transfer was adjusted so that the antenna* population decayed with lifetime $\tau_1 = 23$ ps. The resulting numerical time-dependent populations for P700*, $P700^+A_0^-$, and $P700^+A_1^-$ were then compared with those computed using eqs 2, with $\tau_1 = 23$ ps, $\tau_2 = 1.3$ ps, and $\tau_3 = 13$ ps. For τ_b between 1 and 5 ps, the populations computed with and without back-transfer agreed to within 5%; for longer τ_b, even closer agreement was obtained. For $\tau_b < 0.5$ ps, the simulation excluding back-transfer fails significantly. In a more realistic model, P700 was surrounded by three antenna Chls; forward and backward energy exchanges were allowed among all four of these species. The P700* → $P700^+A_0^-$ and $A_0^- \rightarrow A_1$ steps were assigned the lifetimes 1.3 and 13 ps; the energy-transfer rates among the antenna Chls and P700 were scaled to yield 23 ps decay in the total antenna excitation population. The populations for P700*, $P700^+A_0^-$, and $P700^+A_1^-$ coincided with those computed from eq 2 to within 5%. Finally, simulations were carried out for electronic energy transfers among antenna and reaction center Chls in the positions and orientations reported by Krauss et al. (*7*); energy transfers were allowed between all Chl pairs. The 0−0 antenna Chl absorption wavelengths were randomly distributed in space, under the constraint that the sum of single-site spectra converges to the experimental PS I absorption spectrum. The P700 and A_0 Chls were assigned the wavelengths 700 and 686 nm; the relative probabilities of forward- and back-transfers were

computed using the pertinent Förster spectral overlap integrals. The P700* → $P700^+A_0^-$ and A_0^- → A_1 electron transfers were represented with time constants $\tau_2 = 1.3$ ps and $\tau_3 = 13$ ps. The Förster energy-transfer rates were scaled by a common factor so that the total antenna excitation populations resulting from solution of the master equations decayed with lifetime $\tau_1 = 23$ ps. The numerical populations of the states P700*, $P700^+A_0^-$, and $P700^+A_1^-$ generated in this simulation conformed closely with eq 2. Hence, the details of the antenna excitation trapping at P700 are not germane to interpretations of reaction center processes—particularly when the trapping time τ_1 is long compared to τ_2. Excitation of the core antenna in PS I with femtosecond laser pulses is essentially equivalent to preparing P700* with a single-sided exponential laser pulse with 23 ps trailing edge, regardless of the physical pathways by which P700* emerges. In this analysis, the lifetime τ_2 only characterizes the kinetics of $P700^+A_0^-$ formation from P700*; it does not necessarily coincide with the intrinsic time constant for the primary charge separation. However, τ_3 directly represents the time scale of the electron-transfer A_0^- → A_1. We note in passing that in experiments with highly enriched PS I reaction centers (in which the reaction center cofactors themseleves may absorb a significant fraction of the pump light), our kinetic model may be inapplicable. We should also empasize that the accuracy of our simple kinetic model stems in part from the fact that the lifetime τ_2 is significantly shorter than the back-transfer time τ_b. It cannot be generalized to systems where back-transfers compete effectively with charge separation.

Our kinetic model appears to be the simplest one that can account for all of the kinetic features in Figure 2. Since it is unknown whether one or both of the PsaA and PsaB branches contribute to the electron transfers in PS I, the model was augmented to allow for involvement of both branches; each branch was accorded independent values of τ_2 and τ_3. The principal conclusion of this modeling was either that both branches exhibit very similar lifetimes and A_0 band spectra, or that electron-transfer proceeds in one branch with >70% efficiency. In the latter case, the lifetimes and A_0 spectrum would essentially be defined by those of the active branch.

To check for effects of Q_y vibrational features on the interpretation of the kinetics in Figure 2, the Gaussian fits to the cofactor spectra in Figures 1 and 3 were convoluted with the 300 K monomeric chlorophyll *a* single-site absorption spectrum. The latter was computed using the 43 known vibrational frequencies (*31*) with Huang−Rhys factors adjusted to fit the experimental single-site profile at 4 K (*32*). The vibrational features of the monomeric Chl cofactors prove to exhibit negligible amplitudes from 680 to 700 nm, relative to those of the vibrationless origin bands. Their effect is marginal at 675 nm. This conclusion is consistent with the fact that the amplitudes of the empirical vibronic features in the ($P700^+$ − P700) difference spectra in Figure 1 are insignificant for wavelengths >675 nm. No attempt was made here to disentangle the vibrational features among reaction center pigments at wavelengths <675 nm.

Hastings et al. (*10*) observed a time-resolved (open − closed) absorption difference profile for *Synechocystis* sp. at 686 nm, which qualitatively resembles our 685 and 690 nm profiles in Figure 2. Since 686 nm falls near the A_0 absorption maximum, and since that profile can be fitted using a ∼4 ps photobleaching rise component combined with a ∼20 ps photobleaching decay, Hastings et al. assigned these kinetic features to formation and decay of A_0^-, respectively. This implied that the 4 ps kinetics arose from trapping at P700 (foreshortened by annihilation at the excitation densities used), while the 20 ps phase was due to the A_0^- → A_1 transfer. This interpretation overlooked the effects of C690 absorption growth and P700* stimulated emission, which are not negligible at 686 nm (cf. Figure 3). In our analysis, the ∼20 ps kinetic component (which corresponds to our τ_1 in the model of eq 1) emerges as a natural consequence of the excitation trapping at P700, which precedes the primary charge separation. No simulation can adequately reproduce the (open − closed) difference profiles in Figure 2, using reasonable cofactor spectra combined with the kinetic scenario proposed by Hastings et al.

Our experiments suggest that the P700 A_0 → $P700^+$ A_0^- process in PS I shows 1−2 ps kinetics. For comparison, White et al. (*33*) reported ∼3 ps (A_0^- − A_0) rise kinetics in PS I from spinach; Kumazaki et al. (*34*) inferred that the intrinsic time constant for the primary electron transfer from P700* in highly enriched PS I particles (∼14 Chls/P700) is less than 4 ps. Earlier estimates of the A_0^- → A_1 electron-transfer kinetics in PS I, which have ranged from 20 to 50 ps (*10, 33, 35*−*37*), may have been influenced by the relatively slow antenna excitation trapping at P700. Brettel and Vos (*35*) observed 30 ps A_1^- formation kinetics by directly probing A_1 absorption in PS I complexes at 380−390 nm. They identified these kinetics with the A_0^- → A_1 process, under the assumption that the time scales for excitation trapping and charge separation are short compared to 30 ps. Since the excitation trapping at P700 was not independently monitored, however, it is unclear to what extent it may have been influenced by annihilation.

The 13 ps A_0^- → A_1 electron transfer in photosystem I is at least an order of magnitude faster than the corresponding H^- → Q_A processes in purple bacteria (*2, 3*). In *Rb. sphaeroides*, for example, single-exponential fits to absorbance changes associated with the latter process yield lifetimes ranging from 80 to 320 ps, depending on probe wavelength. (This complexity may arise from a distribution of conformational states in such reaction centers.) A large disparity between PS I and purple bacteria is not surprising, because the 4.5−5 Å edge−edge separation between the primary acceptor A_0 and the phylloquinone A_1 in PS I (*38*) is ∼5 Å smaller than that between H and Q_A in *Rb. sphaeroides* (9.6 Å). However, our A_0^- → A_1 electron-transfer rate in photosystem I is considerably slower than the 0.8 ps kinetics predicted by the Moser−Dutton "ruler" (*39*), under the assumption that the electron transfer occurs in the "optimal" regime where $\Delta G°$ matches the reorganization energy λ that accompanyies the electron transfer. Hence, it appears likely either that the A_0^- → A_1 electron transfer in PS I occurs in the "normal" or "inverted" regimes, or that other assumptions underlying the original Moser−Dutton relationship do not hold in PS I.

REFERENCES

1. Zinth, W., and Kaiser, W. (1993) in *The Photosynthetic Reaction Center* (Deisenhofer, J., and Norris, J., Eds.) Vol. II, pp 71−88, Academic Press, London.
2. Kirmaier, C., and Holten, D. (1990) *Proc. Natl. Acad. Sci. U.S.A. 87*, 3552−3556.

3. Woodbury, N. W., and Allen, J. P. (1995) in *Anoxygenic Photosynthetic Bacteria* (Blankenship, R. E., Madigan, M. T., and Bauer, C. E., Eds.) pp 527−557, Kluwer, Dordrecht, The Netherlands.
4. Allen, J. P., Feher, G., Yeates, T. O., Rees, D. C., Deisenhofer, J., Michel, H., and Huber, R. (1986) *Proc. Natl. Acad. Sci. U.S.A. 83*, 8589−8593.
5. Chang, C.-H., El-Kabbani, O., Tiede, D., Norris, J., and Schiffer, M. (1991) *Biochemistry 30*, 5352−5360.
6. Krauss, N., Hinrichs, W., Witt, I., Fromme, P., Pritzkow, W., Dauter, Z., Betzel, C., Wilson, K. S., Witt, H. T., and Saenger, W. (1993) *Nature 361*, 326−331.
7. Krauss, N., Schubert, W.-D., Klukas, O., Fromme, P., Witt, H. T., and Saenger, W. (1996) *Nat. Struct. Biol. 3*, 965−973.
8. Müller, M. G., Hucke, M., Reus, M., and Holzwarth, A. R. (1996) *J. Phys. Chem. 100*, 9527−9536; and references cited therein.
9. Savikhin, S., Xu, W., Soukoulis, V., Chitnis, P. R., and Struve, W. S. (1999) *Biophys. J. 76*, 3278−3288.
10. Hastings, G., Kleinherenbrink, F. A. M., Lin, S., and Blankenship, R. E. (1994) *Biochemistry 33*, 3193−3200.
11. Nuijs, A. M., Shuvalov, V. A., van Gorkom, H. J., Plijter, J. J., and Duysens, L. N. M. (1986) *Biochim. Biophys. Acta 850*, 310−318.
12. Shuvalov, V. A., Nuijs, A. M., van Gorkom, H. J., Smit, H. W., and van Duysens, L. N. M. (1986) *Biochim. Biophys. Acta 850*, 319−323.
13. Owens, T. G., Webb, S. P., Alberte, R. S., Mets, L., and Fleming, G. R. (1988) *Biophys. J. 53*, 733−745.
14. Klug, D. R., Giorgi, L. B., Crystal, B., Barber, J., and Porter, G. (1989) *Photosynth. Res. 22*, 277−284.
15. Turconi, S., Schweitzer, G., and Holzwarth, A. R. (1993) *Photochem. Photobiol. 57*, 113−119.
16. Savikhin, S., Xu, W., Chitnis, P. R., and Struve, W. S. (2000) *Biophys. J. 79*, 1573−1586.
17. Byrdin, M., Rimke, I., Schlodder, E., Stehlik, D., and Roelofs, T. (2000) *Biophys. J. 79*, 992−1007.
18. Sun, J., An, K., Jin, P., Chitnis, V. P., and Chitnis, P. R. (1998) *Methods Enzymol. 297*, 124−139.
19. Hiyama, T., and Ke, B. (1971) *Arch. Biochem. Biophys. 147*, 99−108.
20. Diaz-Quintana, A., Leibl, W., Bottin, H., and Setif, P. (1998) *Biochemistry 37*, 3429−3439.
21. Hasson, K. C. (1997) Ph.D. Thesis, Harvard University, Cambridge, MA.
22. Schaffernicht, H., and Junge, W. (1981) *Photochem. Photobiol. 34*, 223−232.
23. Hervas, M., Ortega, J. M., Navarro, J. A., De la Rosa, M. A., and Bottin, H. (1994) *Biochim. Biophys. Acta 1184*, 235−241.
24. Hippler, M., Drepper, F., Farah, J., and Rochaix, J.-D. (1997) *Biochemistry 36*, 6343−6349.
25. Gillie, J. K., Lyle, P. A., Small, G. J., and Golbeck, J. H. (1989) *Photosynth. Res. 22*, 233−246.
26. Hastings, G., Hoshina, S., Webber, A. N., and Blankenship, R. E. (1995) *Biochemistry 34*, 15512−15522.
27. Fujita, I., Davis, M. S., and Fajer, J. (1978) *J. Am. Chem. Soc. 100*, 6280−6282.
28. Johnson, T. W., Shen, G., Zybailov, B., Kolling, D., Reategui, R., Beauparlant, R. S., Vassiliev, I. R., Bryant, D. A., Jones, A. D., Golbeck, J. H., and Chitnis, P. R. (2000) *J. Biol. Chem. 275*, 8523−8530.
29. Semenov, A. Yu., Vassiliev, I. R., van der Est, A., Mamedov, M. D., Zybailov, B., Shen, G., Stehlik, D., Diner, B. A., Chitnis, P. R., and Golbeck, J. H. (2000) *J. Biol. Chem. 275*, in press.
30. Rätsep, M., Johnson, T. W., Chitnis, P. R., and Small, G. J. (2000) *J. Phys. Chem. B104*, 836−847.
31. Gillie, J. K., Small, G. J., and Golbeck, J. H. (1989) *J. Phys. Chem. 93*, 1620−1627.
32. Peterman, E. J. G., Pullerits, T., van Grondelle, R., and van Amerongen, H., (1997) *J. Phys. Chem. B101*, 4448.
33. White, N. T. H., Beddard, G. S., Thorne, R. G., Feehan, T. M., Keyes, T. E., and Heathcote, P. (1996) *J. Phys. Chem. 100*, 12086−12099.
34. Kumazaki, S., Ikegami, I., and Yoshihara, K. (1997) *J. Phys. Chem. A101*, 597−604.
35. Brettel, K., and Vos, M. H. (1999) *FEBS Lett. 447*, 315−317.
36. Iwaki, M., Kumazaki, S., Yoshihara, K., Erabi, T., and Itoh, S. (1995) in *Photosynthesis: from Light to Biosphere* (Mathis, M., Ed.) Vol. 2, pp 147−150, Kluwer, Dordrecht, The Netherlands.
37. Kumazaki, S., Iwaki, M., Ikegami, I., Kandori, H., Yoshihara, K., and Itoh, S. (1994) *J. Phys. Chem. 98*, 11220−11225.
38. Klukas, O., Schubert, W.-D., Jordan, P., Krauss, N., Fromme, P., Witt, H. T., and Saenger, W. (1999) *J. Biol. Chem. 274*, 7361−7367.
39. Moser, C. C., Keske, J. M., Warncke, K., Farid, R. S., and Dutton, P. L. (1992) *Nature 355*, 796−802.

BI0104165